

Article

Biogeochemistry and Water–Rock Interactions of Coalbed Methane Co-Produced Water in the Shizhuangnan Block of the Southern Qinshui Basin, China

Yang Li ^{1,2,3} , Shuheng Tang ^{1,2,3,*}, Songhang Zhang ^{1,2,3}, Zhaodong Xi ^{1,2,3} and Pengfei Wang ^{1,2,3}

¹ School of Energy Resource, China University of Geosciences, Beijing 100083, China; liyangly@cugb.edu.cn (Y.L.); zhangsh@cugb.edu.cn (S.Z.); xizhaod@cugb.edu.cn (Z.X.); wpengfei@cugb.edu.cn (P.W.)

² Key Laboratory of Marine Reservoir Evolution and Hydrocarbon Enrichment Mechanism, Ministry of Education, Beijing 100083, China

³ Key Laboratory of Strategy Evaluation for Shale Gas, Ministry of Land and Resources, Beijing 100083, China

* Correspondence: tangsh@cugb.edu.cn; Tel.: +86-10-8232-2005

Received: 19 November 2019; Accepted: 25 December 2019; Published: 31 December 2019



Abstract: Coalbed methane is a major unconventional resource that has been exploited commercially for decades in the southern Qinshui Basin of China. The hydrogeochemical characteristics of coal reservoir water play a key role in the exploration and development of coalbed methane resources. In view of this, a detailed study was performed on coalbed methane co-produced water collected from the Shizhuangnan block to assess water–rock interactions and biogeochemical processes. Water samples were analyzed to establish major ions, isotopic compositions and perform 16S rRNA sequencing. Results suggest that the hydrochemistry was controlled by water–rock processes and that methane was consumed by sulfate reduction through calculation. Meanwhile, the isotopic compositions of water samples indicated that they had a predominantly meteoric origin and were influenced by microbial activity. The 16S rRNA sequencing results of bacteria and archaea provide an important foundation for understanding the activity of sulfate-reducing bacteria and methanogens at different hydraulic heads, which was consistent with isotopic analysis. Carbonates containing calcite and dolomite were found to be distributed at different hydraulic head due to the biogeochemical characteristics and associated water–rock interactions.

Keywords: coal bed methane; hydraulic head; biogeochemistry; sulfate reducing bacteria; methanogens

1. Introduction

As a low-pressure gas reservoir, most coalbed methane (CBM) is thought to be adsorbed on the surface area of coal micropores, which needs lower reservoir pressure below desorption pressure through reducing coalbed reservoir water, forming a pressure drop funnel [1]. As a result, the gas from the coal micropores is released into the cleat system and well bore. The water is extracted from confined coal reservoirs in which adjacent layers are impermeable, resulting in difficult movement across these layers [2]. The water discharged from a CBM well is referred to as CBM co-produced water. Analysis of geochemical compositions of CBM co-produced water is necessary to understand the evolution processes and water–rock interactions along the flow paths. CBM co-produced water usually contains several important ions, with Na^+ , K^+ , Ca^{2+} , Mg^{2+} , Cl^- , HCO_3^- , CO_3^{2-} , and SO_4^{2-} accounting for most

of the total solute in groundwater [3]. Generally, shallow coal seam water is characterized by runoff areas with higher Ca^{2+} , Mg^{2+} , and SO_4^{2-} contents and lower Na^+ , K^+ , and HCO_3^- contents, whereas deep coal seam water is characterized by stagnant areas with lower Ca^{2+} , Mg^{2+} , and SO_4^{2-} contents and higher Na^+ , K^+ , and HCO_3^- contents, as shown in several significant CBM production blocks such as Surat Basin and Powder River Basin [4].

It is intelligible that ubiquitous microbial communities survive in natural environments and are involved in geochemical cycles [5]. In CBM research, the concept of biogenic gas was established in the 1980s. Anaerobic methanogens belonging to archaea were potentially responsible for the earliest form of energy metabolism on earth, about 3.5 billion years ago [6]. According to metabolic pathways of archaeal methanogens, biogenic gas types have been classified as CO_2 reduction and acetate fermentation. Studies carried out since have shown that biogenic gas exists in various CBM production regions worldwide [7].

Sulfate-reducing bacteria are primary microbes controlling methane oxidation, with an increasing body of evidence confirming their importance in the global carbon and sulfur cycles [8]. A large number of sulfate-reducing bacteria responsible for methane oxidation have been identified in marine and lake sediments [9]. It is estimated that worldwide about 90% of methane is consumed by anaerobic oxidation of methane (AOM) [10,11].

Previous studies have revealed that an influx of meteoric recharge and surface water introduces and stimulates microbial communities in shallow coal reservoirs, resulting in coal reservoir water systems being ideal to study the role of biogeochemical processes [12]. In coal reservoir water, the injection of meteoric water and organic material enable the system to have abundant microbes [13]. Hence, the microbial analysis based on biogeochemical characteristics in coal reservoirs is essential to comprehend the relationship between microbes and environments.

The southern Qinshui Basin is a highly productive coalbed methane commercial development region in China, containing Chengzhuang, Fanzhuang, Panzhuang, Shizhuangbei, Shizhuangnan, and Zhengzhuang (Figure 1). At present, one of the most important CBM blocks developed in the southern Qinshui Basin is the Shizhuangnan block, which has more than 1500 drainage wells [14]. The geological structure and hydrological conditions of the study area are suitable for the occurrence of CBM, with a distinct redox boundary that is favorable for the growth of various microbes. In the south of the Qinshui Basin, Guo et al., 2014 reported the presence of CO_2 reduction methanogens through laboratory microbial enrichment culture analysis [15]. Additionally, Yang et al., 2018 employed lump anthracite amendment with coal reservoir water as an inoculum to realize industrialized CBM production, suggesting that CO_2 reduction methanogens are main archaea [16]. However, few studies have focused on archaeal methanogens and associated bacteria in situ, or assessed the relationship between microbial community structure and geochemical characteristics in the southern Qinshui Basin. In this study, the stable isotopic compositions, major and minor ions in CBM co-produced water, were analyzed. Moreover, the microbial species in the coal reservoir water at varying depths by 16S rRNA sequencing were investigated to evaluate microbial effects in the Shizhuangnan block.

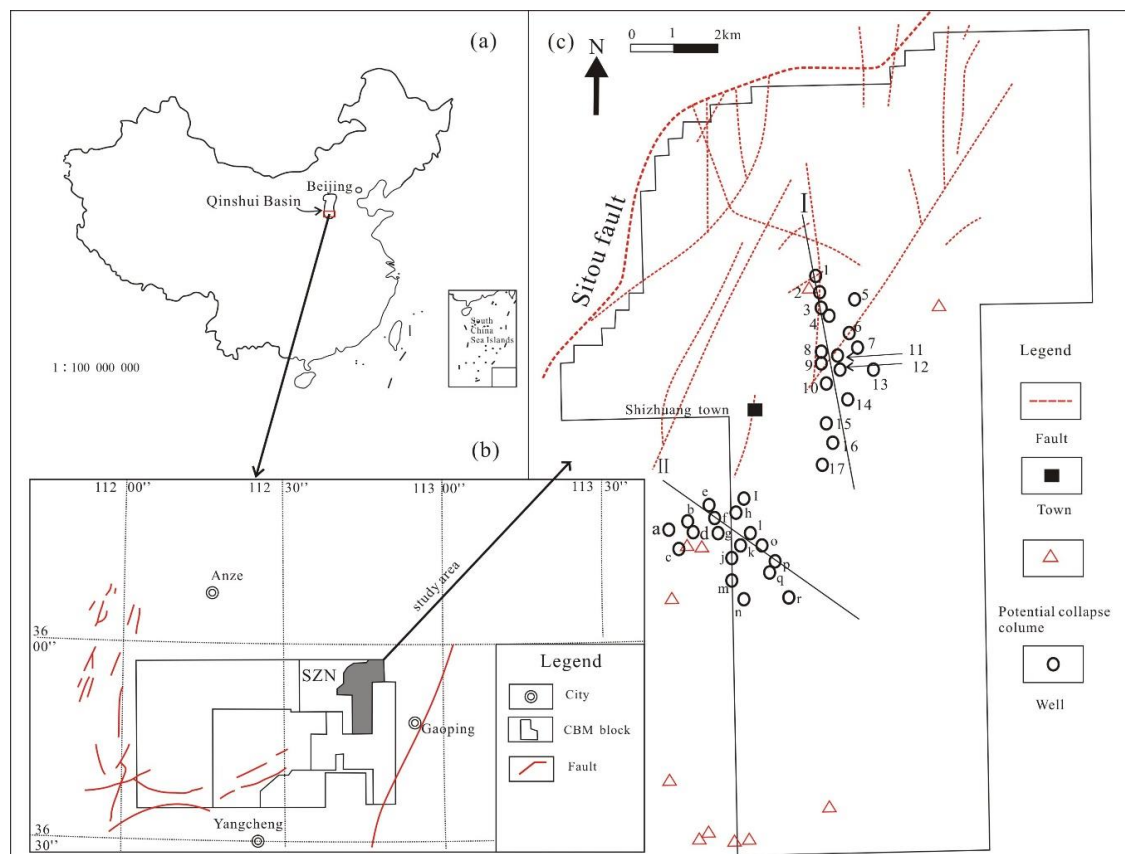


Figure 1. Location of study area and sampling sites: (a) location of the Qinshui Basin in China; (b) location of the Shizhuangnan block in the Qinshui Basin (SZN, the Shizhuangnan block); (c) location of sampling sites in the Shizhuangnan block.

2. Geological Settings

The Qinshui Basin is located in the southeast of Shanxi Province, covering a total area of more than 30,000 km². The elevation of the basin is mostly around 700 m with an undulating topography caused by significant cutting. Central and southern Qinshui Basin are the largest coal bearing regions in Shanxi Province, containing extremely rich coal resources. This area is known for high quality coal production, and is also the first basin to be used for CBM exploration and development in China [17].

The Shizhuangnan block is situated in the southeast region of the Qinshui Basin in the northwest inclined slope belt. The largest fault developed in the western region is the Sitou normal fault, which runs in a northeastern direction with a large extension length. The coal bearing strata in the south of Qinshui Basin include the Benxi formation, Taiyuan formation, Shanxi formation, and Xiashihezi formation, among which the Benxi formation and Xiashihezi formation only contain thin coal seams and have no significant economic mining value. The Taiyuan and Shanxi formations are the main coal bearing strata, with coal seam no. 3 in the lower part of the Shanxi formation being the target seam in the present study [18].

The hydrogeological conditions in the study area are relatively simple, with complete recharge, runoff, and discharge areas. An independent coal aquifer system is formed between the vertical aquifers with weak hydraulic connections caused by the inter-layer runoff and the shale water-separating layer. The sandstone fissure-confined water aquifer of the Shihezi and Shanxi formations is buried deep within the lower Permian layer, characterized by a lithology of medium and fine-grained sandstone, which is the main source of water for coal seam no. 3 in the study area [19].

The Shizhuangnan block groundwater has weak external hydrodynamic impacts, with the deep depth causing groundwater to flow slowly. The whole structure of the Shizhuangnan block is monocline,

dipping to the west. The outcrop of the Jinhua fault on the eastern edge of the basin has a relatively high terrain. After receiving atmospheric precipitation and surface runoff on the eastern side, water flows to the west and supplies the coal reservoir, resulting in various regions, with a runoff region progressing to a transitional region and finally a stagnant region (Figure 2). The Sitou fault on the western side of the Shizhuangnan block forms a natural barrier (Figure 1).

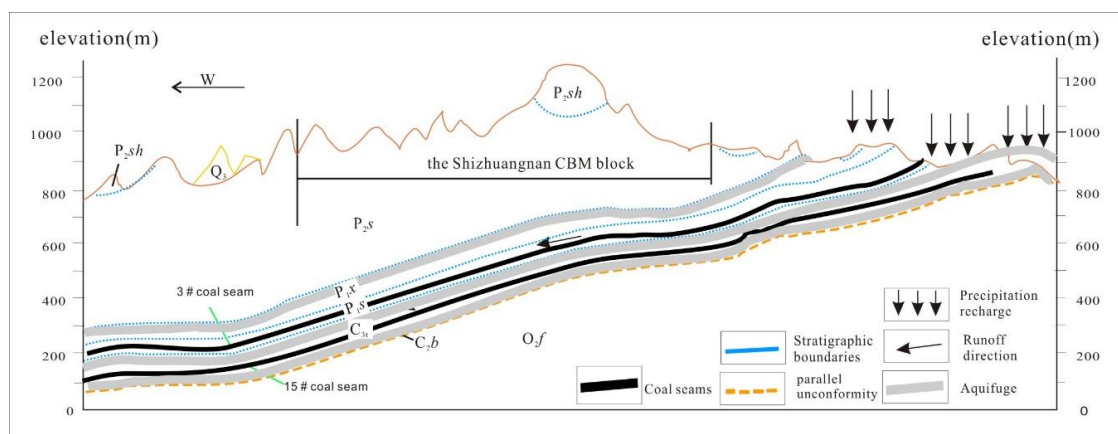


Figure 2. Hydrogeological conditions in the Shizhuangnan block of the Qinshui Basin. CBM: coalbed methane.

3. Materials and Methods

3.1. Sample Site and Collection

All selected CBM wells functioned with a stable production period of more than three years and all CBM co-produced water came from coal seam no. 3. The distribution of sampling sites roughly formed two lines in north (I) and mid-west (II) directions, as shown in Figure 1. Overall, the two lines were arranged from high to low, according to the hydraulic gradient.

Water samples for ion and isotope analysis and 16S rRNA sequencing were collected directly from the CBM wellhead in 5 L bottles and 50 mL centrifuge tubes. The sampling containers were rinsed with the water samples three times. During collection, the whole container was filled with the water, which was then immediately cap sealed. In order to avoid the effect of stagnant water in the drainage pipe, all CBM co-produced water samples were collected from the CBM wells with relatively steady and massive water drainage. Due to uninterrupted water and gas production, it can be considered that the CBM co-produced water was derived from coalbed reservoirs.

To determine the relationship between geochemical data and water source depth, an estimation of the hydraulic head (H) of the CBM reservoir was established, as described in Equation (1):

$$H = H_C - H_L + h_C \quad (1)$$

where H_C is the depth of the coal seam, H_L is the depth of the water level produced initially in the CBM well, and h_C is the elevation of the coal seam. The calculated H represents the hydraulic head of the targeted coal aquifer, with the direction of groundwater flow determined by the H value across the study area, as groundwater flows from high H to low H regions [20,21].

3.2. Analysis of Water Chemical Characteristics

Cations were measured by inductance-coupled plasma emission spectrometry (NEXION-300X), and anions were measured by ion chromatography (Optima 8300) in water samples. A stable isotope mass spectrometer (Thermo Delat V Advantage) was used for analysis of hydrogen and oxygen isotopes and dissolved inorganic carbon isotopes, carbon and hydrogen isotopes of dissolved methane

in water samples. The chemical and isotopic results of CBM co-produced water from the Shizhuangnan block region are shown in Table 1.

Table 1. Dissolved ions, isotopic results, and hydraulic head (H) of CBM co-produced water samples from the Shizhuangnan block.

Well	Cl ⁻ (mg/L)	CO ₃ ²⁻ (mg/L)	HCO ₃ ⁻ (mg/L)	Na ⁺ (K ⁺) (mg/L)	SO ₄ ²⁻ (mg/L)	Ca ²⁺ (mg/L)	Mg ²⁺ (mg/L)	δD (‰)	δ ¹⁸ O (‰)	δ ¹³ CDIC (‰)	H (m)
1	54.17	19.22	573.56	262.56	0.00	2.02	0.61	-80.25	-11.42	27.60	527
2	157.50	21.49	536.81	321.92	1.50	2.20	0.60	-70.16	-10.23	20.23	604
3	112.194	31.20	656.55	335.91	0.28	1.73	0.94	-74.53	-10.88	26.87	609
4	220.88	60.01	905.50	528.13	0.33	2.00	1.00	-74.68	-10.69	19.34	667
5	193.57	33.62	873.77	479.78	3.40	2.37	0.86	-75.48	-11.12	16.00	685
6	201.75	21.60	490.58	337.27	5.04	2.74	0.89	-74.80	-11.12	0.75	689
7	182.50	30.83	312.71	257.12	9.10	3.20	1.10	-80.94	-11.66	-15.46	697
8	78.11	46.10	396.52	240.93	12.60	2.40	2.90	-83.38	-11.79	-17.74	709
9	329.92	40.47	426.32	404.42	11.90	4.10	0.24	-88.06	-11.96	-14.43	710
10	94.31	17.60	466.81	257.83	13.90	3.80	4.40	-82.83	-11.22	-12.45	716
11	167.27	72.01	827.39	476.41	1.05	1.54	2.51	-72.58	-10.95	-10.37	724
12	52.04	31.10	986.02	422.94	13.60	4.21	2.20	-89.35	-12.67		725
13	79.21	28.52	713.34	338.92	17.20	3.80	3.80	-88.13	-12.47		734
14	230.11	19.00	735.43	440.51	12.60	3.80	3.50	-90.26	-12.59		735
15	141.32	47.53	231.61	216.82	18.10	3.00	4.00	-91.15	-12.69		743
16	155.31	28.02	282.82	236.32	18.90	2.30	2.93	-93.14	-12.87		749
17	158.31	47.10	867.32	461.31	12.80	2.90	3.90	-92.97	-12.76		755
a	81.34	38.41	588.21	299.18	0.00	2.57	0.61	-69.63	-11.04	19.16	483
b	55.99	60.03	378.31	223.59	0.43	1.23	1.66	-69.29	-10.53	19.38	511
c	55.91	12.02	683.39	298.37	0.00	2.17	0.82	-77.81	-11.31	15.55	613
d	144.41	39.45	1005.42	329.12	0.60	2.80	0.73	-75.70	-11.00	15.90	614
e	109.75	33.61	746.85	374.55	0.31	2.27	1.27	-84.93	-11.30	11.82	670
f	39.03	26.40	722.44	316.31	0.56	1.83	1.69	-73.68	-11.11	6.70	673
g	81.77	40.81	690.72	341.93	0.30	2.06	0.72	-76.17	-11.16	13.75	676
h	205.50	39.30	690.04	419.71	1.90	1.90	1.40	-90.00	-12.60	7.50	677
i	80.24	24.02	368.54	208.94	7.62	1.92	1.54	-68.14	-10.79	-13.04	701
j	433.52	57.30	878.22	652.32	7.50	4.20	0.92	-89.98	-12.67	-10.67	709
k	88.61	32.13	609.63	312.62	10.40	2.30	3.50	-87.06	-12.35	-11.52	740
l	294.12	10.80	637.62	285.43	9.50	3.60	6.01	-90.08	-12.79	-9.82	743
m	112.71	68.75	540.60	325.22	7.90	2.90	3.50	-80.60	-12.70	-14.50	750
n	186.14	28.40	692.71	400.61	11.50	4.42	3.60	-92.89	-12.85		757
o	129.62	28.45	552.31	310.42	10.30	2.10	3.40	-89.17	-12.91		767
p	738.07	50.12	594.92	736.33	13.60	3.00	3.00	-87.92	-12.68		774
q	226.91	13.50	767.03	478.51	10.30	1.70	6.90	-85.79	-11.89		777
r	78.52	0.01	856.61	368.53	12.40	3.80	3.20	-91.58	-12.77		779

3.3. Gene Extraction, PCR Amplicon, and Sequencing Analysis

Water samples obtained from the CBM well for gene sequencing were stored in an incubator filled with dry ice under a low temperature condition (0–5 °C) while being transferred to the laboratory. To ensure the preservation of complete microbial populations, genes were extracted from the water samples using a FastDNA SPIN Kit according the manufacturer’s instructions within a week after sampling the water. The genes were used as a template for the fusion primer polymerase chain reaction (PCR). The 16S V4 amplicon primers were 515F (GTGCCAGCMGCCGCGGTAA) and 806R (GGACTACHVGGGTWTCTAAT). PCR amplifications were performed using an automatic thermal cycler (PTC-200, Bio-Rad Laboratories; Hercules, CA, USA) and the qualities of the amplified PCR were checked by electrophoresis in 1% agarose gel.

Cluster preparation and sequencing were carried out using qualified libraries. The Illumina Miseq system was used for sequence analysis (Illumina Hiseq or Miseq, San Diego, CA, USA). After sequencing, the samples were differentiated by barcode sequences and each sequence read was quality checked. Low complexity sequences, poor quality reads, and linker sequences were removed. Errors in the sequences after removal of the preprocessed targets were corrected using Mothur pre.cluster software. Using chimeras, chimeric sequences were removed. Low complexity sequences were removed and similar sequences were clustered into operational taxonomic units (OTUs) at 97%

similarity, allowing sample species abundance and diversity analysis to be performed on the basis of OTUs. Classified software was used to perform species classification on postprocessed sequences. Chao, Ace, Shannon, and Simpson indices were calculated using Mothur. The relative abundance was calculated by rarefaction analysis.

4. Results and Discussion

4.1. Geochemical Composition and Water–Rock Interaction

The concentrations of Na^+ (K^+) in the CBM co-produced water ranged from 208.94 to 736.30 mg/L, with an average of 362.87 mg/L, whereas the concentrations of Cl^- ranged from 39.03 to 738.00 mg/L, with an average of 176.41 mg/L. Milligram equivalent of the main water ions was used to determine the source of major ions and hydrogeochemical processes. Dissolution of minerals controls the chemical composition of CBM co-produced water. Similarly, the degree of cation exchange affects geochemical variability in groundwater [22].

Dissolution of halite (NaCl) or sylvite (KCl) is the main source of Na^+ or K^+ in coal reservoir water. Additionally, weathering of silicates such as sodium plagioclase and potash plagioclase release Na^+ or K^+ , respectively. Except for mineral dissolution, secondary processes such as cation exchange between Ca^{2+} or Mg^{2+} and Na^+ or K^+ can increase content of Na^+ and K^+ by reducing Ca^{2+} or Mg^{2+} .

As shown in Figure 3a, the higher milligram equivalent values of Na^+ and K^+ compared with Cl^- in the CBM co-produced water suggest that halite and sylvite were not the only source of Na^+ or K^+ , with silicate weathering and ion exchange potentially being other important factors in the study area [23].

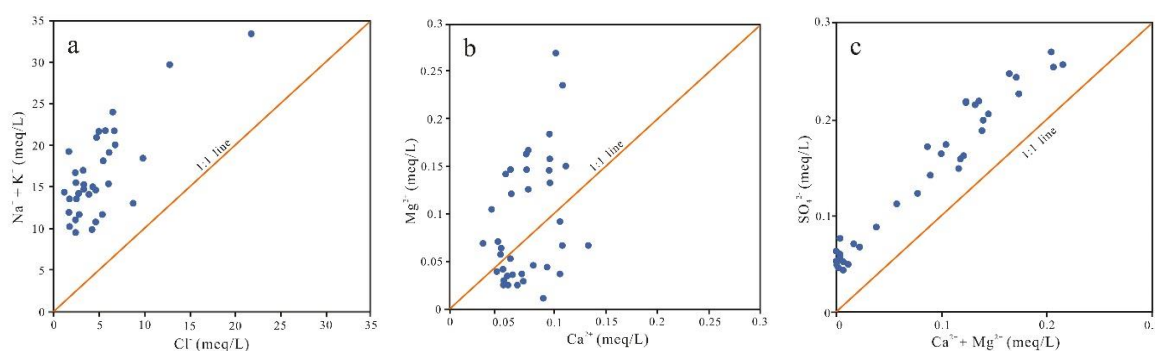
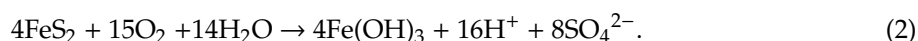
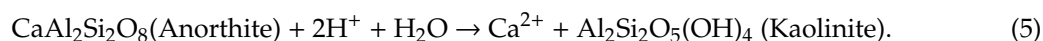
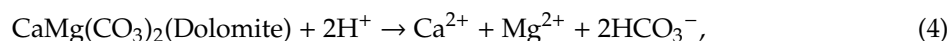


Figure 3. Relationship between hydrochemical characteristics in the Shizhuangnan block: (a) K^+ + Na^+ versus Cl^- ; (b) Mg^{2+} versus Ca^{2+} ; (c) SO_4^{2-} versus Ca^{2+} + Mg^{2+} .

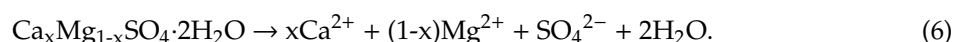
Ca^{2+} , Mg^{2+} , HCO_3^- , and SO_4^{2-} originate from the dissolution of several minerals. The oxidation of sulphide minerals such as pyrite near the surface might increase the amount of SO_4^{2-} and H^+ in coal reservoir water [24], as described by Equation (2):



H^+ would react with carbonate and silicate, releasing Ca^{2+} , Mg^{2+} , and HCO_3^- according to the sequence described in Equations (3)–(5):



In addition, dissolution of gypsum releases Ca^{2+} , Mg^{2+} , and SO_4^{2-} , as described in Equation (6):



The concentrations of Ca^{2+} in the CBM co-produced water ranged from 1.23 to 4.42 mg/L, with an average of 2.71 mg/L. The concentrations of Mg^{2+} ranged from 0.20 to 6.90 mg/L, with an average of 2.31 mg/L. In coal reservoir water, $\text{Ca}^{2+}/\text{Mg}^{2+}$ milligram equivalent is mainly controlled by water-rock interactions. If the milligram equivalent ratio value of $\text{Ca}^{2+}/\text{Mg}^{2+}$ is close to 1, weathering of dolomite is indicated as the dominant source in the coal reservoir, whereas a high milligram equivalent ratio value of $\text{Ca}^{2+}/\text{Mg}^{2+}$ (>1) indicates a greater calcite contribution, and a ratio value greater than 2 indicates that silicate dissolution would take place [25]. In the study area, the milligram equivalent ratio values of $\text{Ca}^{2+}/\text{Mg}^{2+}$ exhibited an obvious positive correlation with each other, suggesting that the dissolution of calcite occurred together with dolomite (Figure 3b).

The milligram equivalent ratio of $\text{Ca}^{2+} + \text{Mg}^{2+}$ over SO_4^{2-} is 1:1 if dissolution of anhydrite or gypsum is also a source of Ca^{2+} , Mg^{2+} , and SO_4^{2-} in CBM co-produced water [3]. As plotted in Figure 3c, a positive correlation was observed in the study area between $\text{Ca}^{2+} + \text{Mg}^{2+}$ and SO_4^{2-} , suggesting that Ca^{2+} , Mg^{2+} , and SO_4^{2-} were derived from anhydrite or gypsum. However, major data points above the 1:1 ratio line show that other water-rock reactions such as the dissolution or precipitation of carbonate, ion exchange, and biogeochemistry also influenced Ca^{2+} , Mg^{2+} , and SO_4^{2-} in the aqueous environment.

The molar ratio of $[(\text{Ca}^{2+} + \text{Mg}^{2+}) - (\text{SO}_4^{2-} + \text{HCO}_3^-)]$ over $[(\text{Na}^+ + \text{K}^+) - \text{Cl}^-]$ is a useful parameter to determine whether cation exchange processes are occurring. The molar ratio value in the study area was close to -1 , indicating the universality of cation exchange between Na^+ (K^+) and $\text{Ca}^{2+}/\text{Mg}^{2+}$ [26]. As plotted in Figure 4a, it is evident that cation exchange was common in the coal reservoir water.

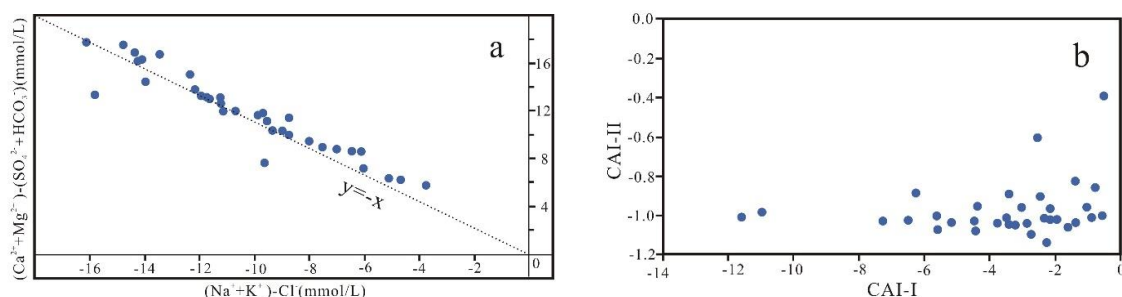


Figure 4. (a) Molar ratio of $(\text{Ca}^{2+} + \text{Mg}^{2+}) - (\text{SO}_4^{2-} + \text{HCO}_3^-)$ versus $(\text{Na}^+ + \text{K}^+) - \text{Cl}^-$; (b) chloro-alkaline indices.

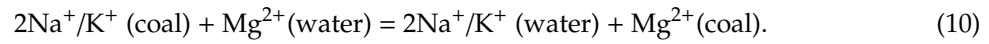
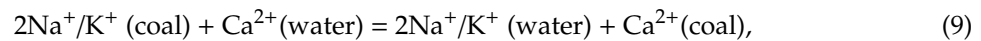
The above analysis confirms the universality of cation exchange in the study area, with the direction and extent of cation exchange being quantified by the chloro-alkaline indices (CAI) during chemical evolution of the coal reservoir water [27]. CAI-1 and CAI-2 are respectively described according to Equations (7) and (8):

$$\text{CAI-1} = [\text{Cl}^- - (\text{Na}^+ + \text{K}^+)]/\text{Cl}^-, \quad (7)$$

$$\text{CAI-2} = [\text{Cl}^- - (\text{Na}^+ + \text{K}^+)]/[\text{SO}_4^{2-} + \text{HCO}_3^- + \text{CO}_3^{2-}]. \quad (8)$$

Ion concentrations are expressed in units of meq/L. When CAI value is positive, Na^+ or K^+ are considered as exchanging with Ca^{2+} and Mg^{2+} in coalbed aqueous environments, whereas a negative CAI value indicates that the inverse reaction occurred. Moreover, the absolute CAI value represents the degree of ion exchange. As described in Figure 4b, the absolute CAI values in the study area were

negative, indicating that Ca^{2+} and Mg^{2+} were removed from the coal aquifer coupled with Na^+ or K^+ entering the solution, according to Equations (9) and (10):



4.2. Formation of Sulfate Profile

SO_4^{2-} concentrations on the two sampling lines (I and II) decreased with decreasing hydraulic head (H) levels (Figure 5a,b), with complete depletion observed by 660 ± 10 m. The SO_4^{2-} concentration profiles are classified as a quasi-straight type pattern. The sulfate gradients for lines I and II were $1.9 \text{ mmol}/(\text{L} \times \text{m})$ and $1.1 \text{ mmol}/(\text{L} \times \text{m})$, respectively.

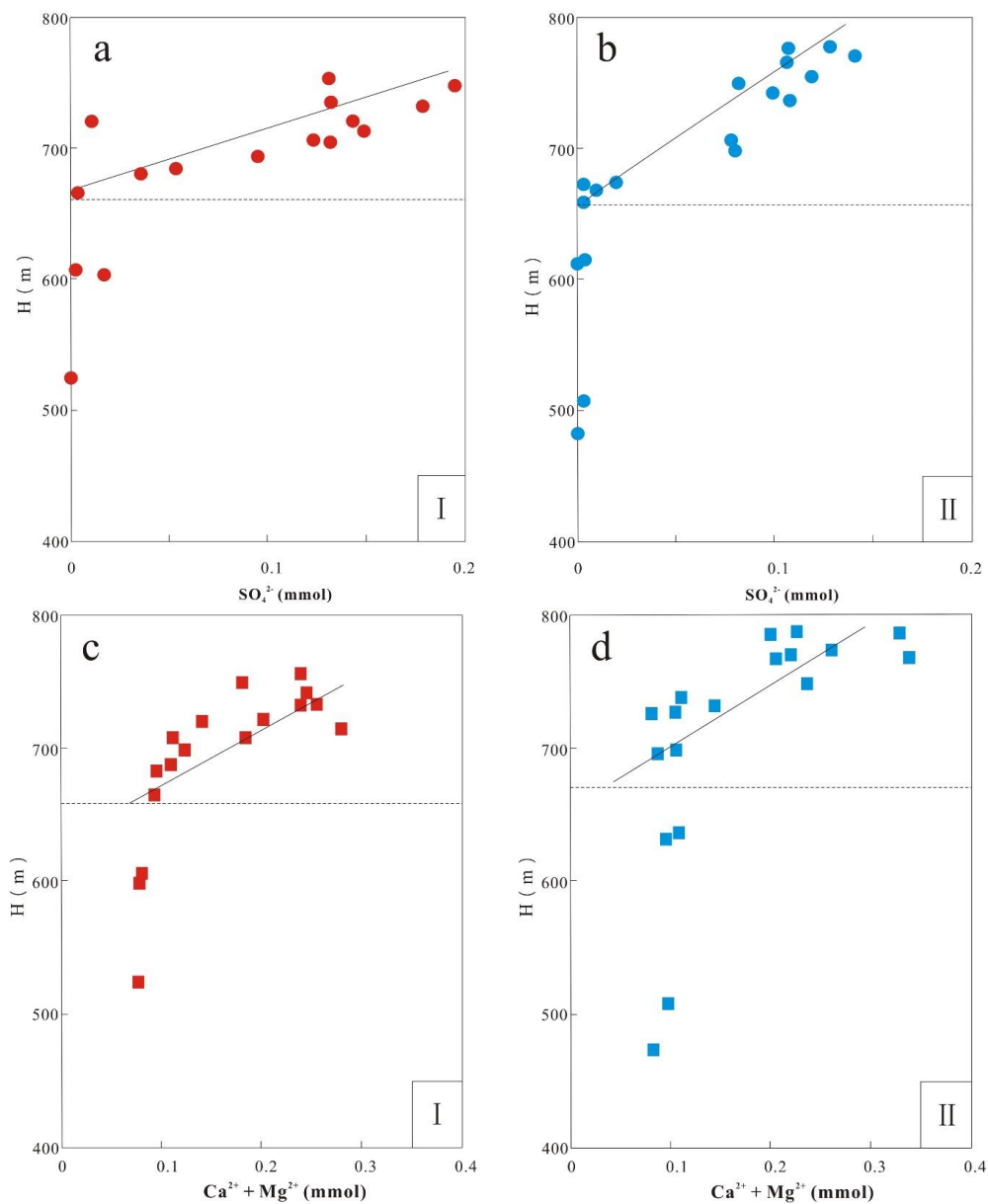
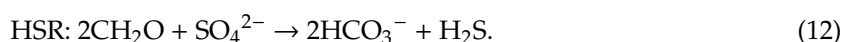


Figure 5. Concentration profiles for SO_4^{2-} (a,b) and the sum of Ca^{2+} and Mg^{2+} (c,d), according to the hydraulic head (H) on the sampling lines I and II.

The concentration profiles of the sum of Ca^{2+} and Mg^{2+} showed similar characteristics to the SO_4^{2-} concentration profiles (Figure 5c,d). Above H levels of 660 ± 10 m, the sum concentrations of Ca^{2+} and Mg^{2+} reduced linearly as H decreased. However, below H levels of 660 ± 10 m, the sum concentrations of Ca^{2+} and Mg^{2+} remained constant across the two sampling lines.

Sulfate reduction is a significant metabolic pathway for bacterial anaerobic oxidation, exerting a significant impact on the global sulfur and carbon cycle [28]. As shown in Equation (11), there is the metabolic process regarding SO_4^{2-} as the electron acceptor and CH_4 as the electron donor in aqueous environment, referred to as anaerobic oxidation of methane (AOM). Also, the other metabolic process regards SO_4^{2-} as the electron acceptor and organic matter as the electron donor, referred to as heterotrophic sulfate reduction (HSR) [29], as shown in Equation (12):



The Ca^{2+} and Mg^{2+} concentration profiles also indicate that the sum of Ca^{2+} and Mg^{2+} concentrations were controlled by the same mechanism that affected SO_4^{2-} and dissolved inorganic carbon (DIC) concentrations. The sum of Ca^{2+} and Mg^{2+} decreased in accordance with decreasing H because HCO_3^- was produced through AOM and HSR, indicating the forming of authigenic carbonate precipitation [30].

The method used in this study could help to identify and quantify the fraction of SO_4^{2-} consumed by AOM ($C_{\text{SO}_4^{2-}\text{-AOM}}$) and HSR ($C_{\text{SO}_4^{2-}\text{-HSR}}$) [31]. It could therefore be assumed that the consumption ratio of SO_4^{2-} in AOM and HSR followed Equations (13) and (14):

$$C_{\text{SO}_4^{2-}\text{-AOM}} + C_{\text{SO}_4^{2-}\text{-HSR}} = \text{total } \text{SO}_4^{2-} \text{ consumption}, \quad (13)$$

$$C_{\text{SO}_4^{2-}\text{-AOM}} + 2C_{\text{SO}_4^{2-}\text{-HSR}} = \text{total DIC production} = \text{total } \text{Ca}^{2+} \text{ and } \text{Mg}^{2+} \text{ consumption}. \quad (14)$$

Here, on account of different quantitative relationships in DIC production and SO_4^{2-} consumption from AOM and HSR, it could be assumed that the consumption of SO_4^{2-} occurred only via AOM and HSR, whereas the production of DIC only occurred via AOM and HSR. In addition, the total DIC produced via AOM and HSR was consumed by authigenic carbonate precipitation. The consumption of SO_4^{2-} and the sum of Ca^{2+} and Mg^{2+} could be estimated by the concentration gradients in the study area, allowing the two unknown values ($C_{\text{SO}_4^{2-}\text{-AOM}}$, $C_{\text{SO}_4^{2-}\text{-HSR}}$) in Equations (13) and (14) to be solved. In the two sampling lines, the concentration gradients of SO_4^{2-} were 1.9 mmol/(L × m) and 1.2 mmol/(L × m), respectively, whereas the concentration gradients of the sum of Ca^{2+} and Mg^{2+} were 2.0 mmol/(L × m) and 1.5 mmol/(L × m), respectively. Therefore, the calculation results showed that the proportions of SO_4^{2-} reduced by AOM were more than 95% and 75% in the two sampling lines (I and II), respectively.

4.3. Methanogenesis and Isotopic Composition

Dissolved inorganic carbon (DIC) is the sum of inorganic carbon components in solution, including carbon dioxide, carbonic acid, bicarbonate, and carbonate. The two main sources of DIC in most groundwater environments are organic degradation and carbonate dissolution [32]. The value of $\delta^{13}\text{C}_{\text{DIC}}$ in most natural water environments is negative, whereas CBM co-produced water associated with methanogenesis commonly has a positive $\delta^{13}\text{C}_{\text{DIC}}$, ranging from +10 to +30‰ [33]. When the concentrations of SO_4^{2-} decrease, the activity of sulfate-reducing bacteria is inhibited while methanogens become more active. Methanogens preferentially utilize ^{12}C , resulting in the enrichment of $\delta^{13}\text{C}_{\text{DIC}}$ in residual coal reservoir water [34]. Methanogenesis has been reported to lead to a positive $\delta^{13}\text{C}_{\text{DIC}}$ value in some coal reservoir basins such as the Alberta Basin, Pennsylvanian Coal, and Powder River Basin [35]. The values of $\delta^{13}\text{C}_{\text{DIC}}$ in the CBM co-produced water samples from the two sampling

lines are shown in Figure 6, with the strongly negative correlation between positive $\delta^{13}\text{C}_{\text{DIC}}$ values and hydraulic head, providing powerful evidence of elevated methanogenesis at deeper depths.

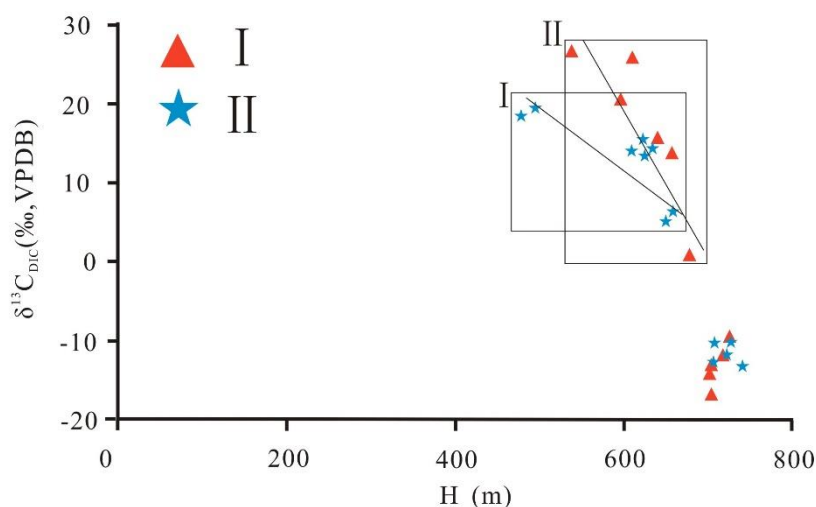


Figure 6. Relationship between $\delta^{13}\text{C}_{\text{DIC}}$ values of dissolved inorganic carbon (DIC) and hydraulic head (H) level in the CBM co-produced water.

The hydrogen and oxygen isotope values near the Chinese meteoric water line (CMWL) and the local meteoric water line (LMWL) illustrate that the CBM co-produced water came from meteoric water (Figure 7) [36]. Hydrogen and oxygen isotopes in groundwater are usually distributed on the right side of the LMWL or CMWL when formed by evaporation, water–rock interaction at high temperature, and mixture with seawater. However, the isotopic compositions on the left side of the LMWL or CMWL are likely modified by methanogenesis, low temperature water–rock interaction, and open system CO_2 exsolution [37]. In the study area, methanogenesis and low temperature water–rock interaction were the main reasons for hydrogen and oxygen isotopes in the water samples falling on the left side of the LMWL or CMWL [38]. Low temperature water–rock interaction, especially precipitation of carbonate in the coal reservoirs, caused the residual water to be depleted in ^{18}O and enriched in D.

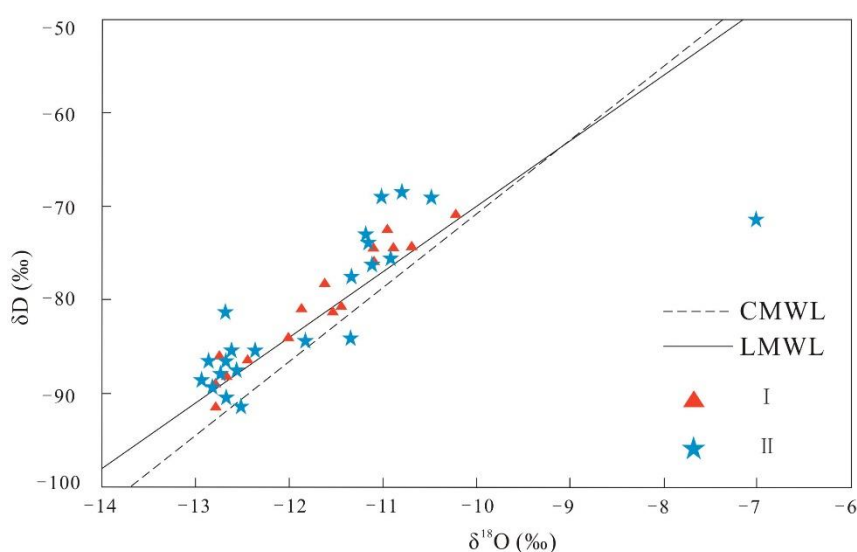
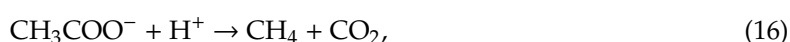


Figure 7. Plot of $\delta\text{d}^{18}\text{O}$ and δD in the water samples. CMWL, China meteoric water line; LMWL, local meteoric water line.

4.4. Microbial Communities Associated with the Methanogenesis and Sulfate Reduction

Previous research under both laboratory and in situ conditions have already proven that underground microbial communities are capable of converting coal into methane [39]. The biodegradation of organic matter is the result of biogeochemistry, which may involve several communities such as degrading bacteria and methanogenic archaea. Generally, coalbed methane is regarded as the end product of methanogenesis in coal seam water, and methanogens are important archaea for the conversion of molecular substrate into methane. The complexity of organic material requires the cooperation of these microbes [40]. However, it is possible that methanogenic archaea have a competitive relationship with some bacteria due to their jointly available substrates. For example, due to the competition between methanogens and sulfate reducing bacteria, the metabolic activity of methanogens would be weakened in the presence of high SO_4^{2-} concentrations [41]. The metabolic modes of methanogenesis can be divided into three categories according to substrate types, namely CO_2 reduction, acetate fermentation, and methylation, as described in Equations (15)–(17):



Proteobacteria are largest at the phylum level with the greatest phylogenetic lineages. *Betaproteobacteria*, *Deltaproteobacteria* and *Gammaproteobacteria* are also usually detected in several significant coal reservoir regions characterized by considerable biogenic methane yield [42]. A majority of known sulfate-reducing bacteria belonging to *Deltaproteobacteria* are capable of degrading naphthalene or other aromatic hydrocarbons [43]. In this study, the focus is on the fact that sulfate-reducing bacteria can limit methanogenic activity under high SO_4^{2-} concentrations resulting from the competitive relationship. In the study region, *Desulfarculales*, *Desulfovibrionales*, *Desulfuromonadales*, and other sulfate-reducing bacteria were detected from the class *Deltaproteobacteria*.

The most common archaea in coal reservoir are *Methanosarcinales*, *Methanomicrobiales*, and *Methanobacteriales* belonging to *Euryarchaeota* at the phylum level. In the water samples, *Methanobacteriales*, *Methanomicrobiales*, and *Methanosarcinales* were detected from the class *Methanobacteria*, which can utilize CO_2 and H_2 rather than acetate to produce biogenic methane [44].

Microbial species in the six coal reservoir water samples at varying hydraulic heads were investigated by 16S rRNA analysis. Relative abundance of *Desulfobacterales*, *Desulfovibrionales*, and *Desulfuromonadales* at the order level are displayed in Figure 8a. Similarly, the relative abundance of *Methanobacteriales*, *Methanomicrobiales*, and *Methanosarcinales* at the order level are displayed in Figure 8b. The relative abundance of methanogens in the CBM co-produced water samples at deep hydraulic head (samples no. 1, 3, a and b) were obviously greater than at shallow hydraulic head (samples no. 4 and 11) as shown in Figure 8b, whereas the relative abundance of sulfate-reducing bacteria followed the opposite trend, as shown in Figure 8a.

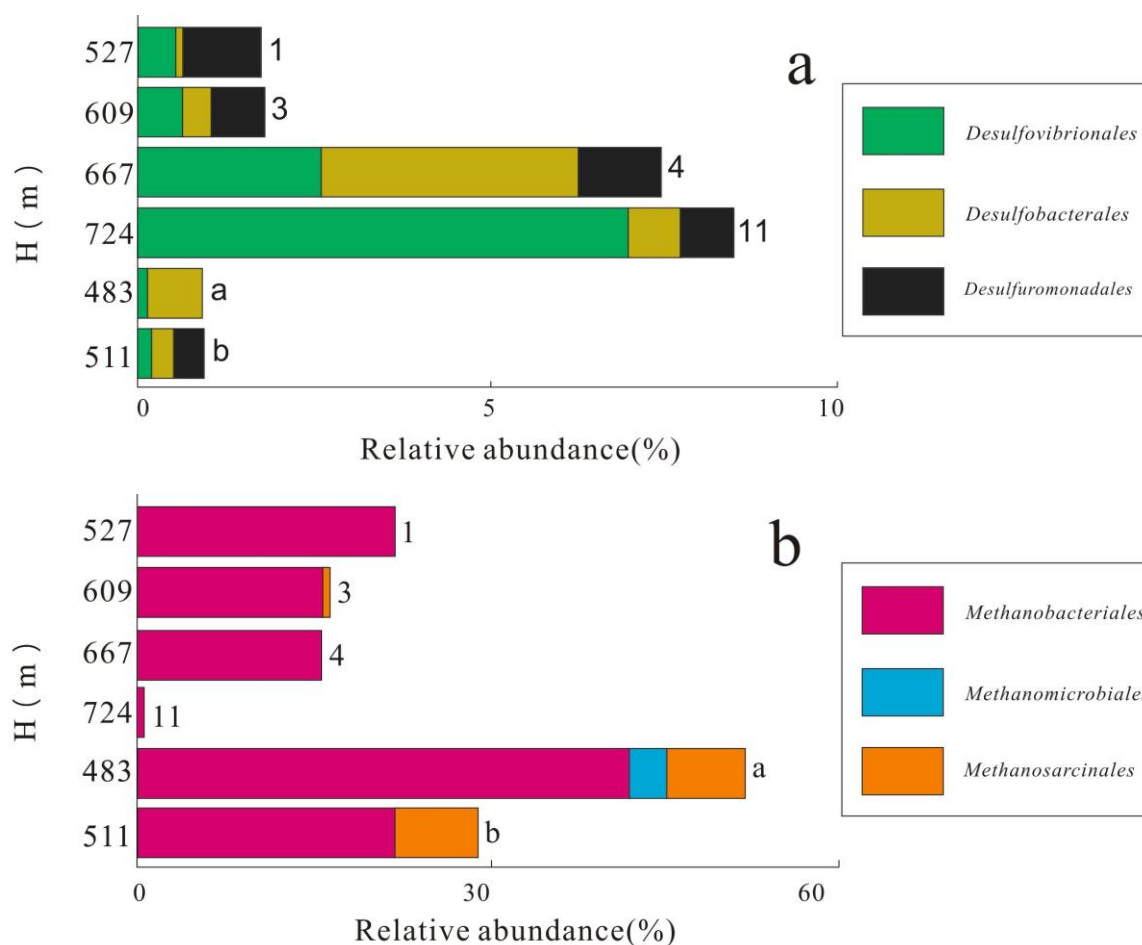


Figure 8. (a) Relative abundance of sulfate reducing bacteria at the order level; (b) relative abundance of methanogens at the order level.

The sequencing results including reads, operational taxonomic units (OTUs), Chao index, Ace index, Shannon index, and Simpson index values from the six water samples are shown in Table 2. Chao index, Ace index, Shannon index, and Simpson index values represent species diversity in a single sample, with larger Chao, Ace, and Shannon index values and smaller Simpson index values indicating that the species in the sample are more abundantly diverse [45]. Combining the species diversity results in Table 2 and the hydraulic head (H) levels in Table 1, the bacterial community including sulfate reducing bacteria at shallow hydraulic head were found to be more abundantly diverse than at deep hydraulic head due to the higher SO_4^{2-} concentrations. Similarly, the archaeal community including methanogens were more abundantly diverse at deep hydraulic head than at shallow hydraulic head, resulting from the depletion of SO_4^{2-} concentrations [46].

The results of the rarefaction curves of the bacterial and archaeal community sequencing for the six water samples are shown in Figure 9. With the increase in sequencing, the accuracy gradually began to improve, and the rarefaction curve began to flatten. The rarefaction curves for all bacterial and archaeal samples illustrated that the characteristics of abundance and diversity are consistent with the results shown in Table 2.

Table 2. Sequencing results of bacterial and archaeal community abundance and diversity indices from the six samples.

Samples	Reads	OTUs	Chao	Ace	Shannon	Simpson
1 (bacteria)	18,655	91	89	96	2.69	0.0990
3 (bacteria)	18,753	104	98	106	2.75	0.0985
4 (bacteria)	21,961	118	120	117	2.91	0.0852
11 (bacteria)	22,252	130	136	135	3.07	0.0712
a (bacteria)	18,127	82	84	90	2.62	0.1096
b (bacteria)	18,367	87	86	91	2.67	0.0995
1 (archaea)	24,123	36	37	37	1.13	0.4177
3 (archaea)	23,979	32	35	34	1.10	0.4358
4 (archaea)	21,980	30	32	33	1.04	0.4557
11 (archaea)	19,576	28	29	30	0.99	0.4778
a (archaea)	24,590	39	41	42	1.21	0.3877
b (archaea)	24,482	37	39	38	1.17	0.3975

OTUs: operational taxonomic units, defined by 97% similarity; Chao: Chao1 estimator; Ace: ACE estimator; Shannon: Shannon diversity index; Simpson: Simpson diversity index.

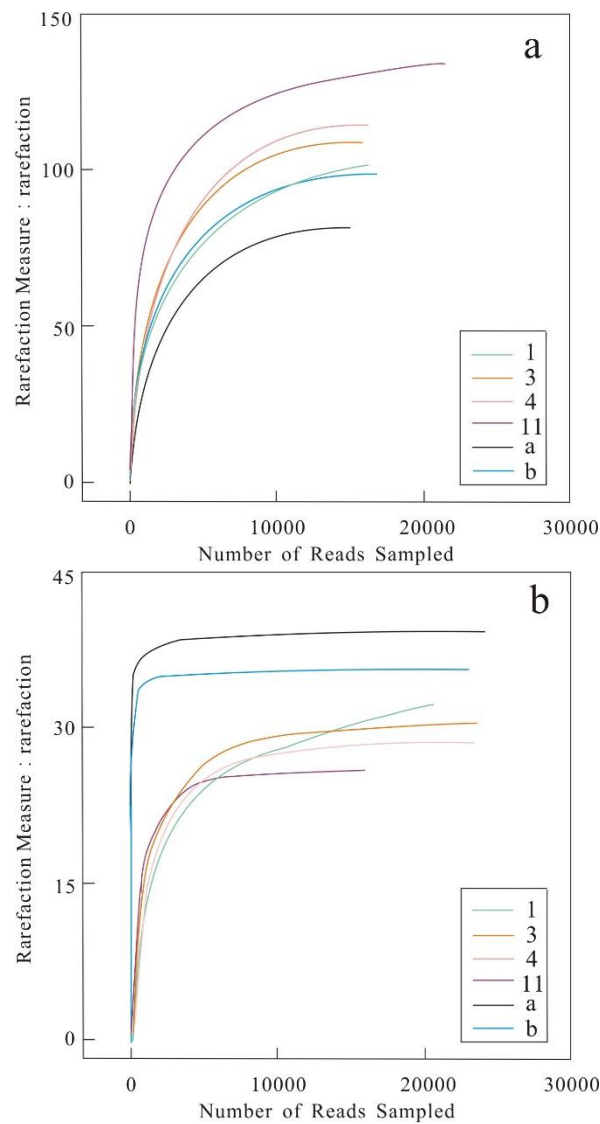


Figure 9. Rarefaction curve of bacteria (a) and archaea (b) from the samples across different wells.

4.5. The Role of Authigenic Carbonate Precipitation

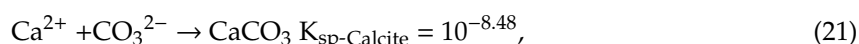
A large amount of DIC is generated by AOM, resulting in authigenic carbonate precipitation [47]. The production of DIC does not necessarily indicate the formation of autogenic carbonate precipitation. Therefore, the ion activity product (IAP) was calculated to ensure the possibility [48]. The rationality of autogenic carbonate precipitation is determined by comparing relative sizes of the solubility product constant (K_{sp}) and IAP. When solution is undersaturated in target coal aquifer ($IAP < K_{sp}$), minerals begin to dissociate, whereas when solution is oversaturated in target coal aquifer ($IAP > K_{sp}$), minerals begin to precipitate. IAP was calculated with the assumption of standard condition (25 °C and standard atmospheric pressure), and therefore the influence of external environmental conditions such as temperature and pressure were ignored [49]. The activity [a] of reactants were calculated by substance concentrations and γ , according to Equations (18)–(20):

$$[a_{Ca^{2+}}] = [Ca^{2+}] \times \gamma_{Ca^{2+}}, \quad (18)$$

$$[a_{Mg^{2+}}] = [Mg^{2+}] \times \gamma_{Mg^{2+}}, \quad (19)$$

$$[a_{CO_3^{2-}}] = [CO_3^{2-}] \times \gamma_{CO_3^{2-}}. \quad (20)$$

The γ values for Ca^{2+} , Mg^{2+} , and CO_3^{2-} were 0.288, 0.248 and 0.207, respectively. For example, $IAP_{Calcite}$ was calculated using Equation (22), and the corresponding calcite precipitation reaction is shown in Equation (21). The values of $IAP_{Calcite}$ and $K_{sp-Calcite}$ were compared to determine whether precipitation reactions occurred, with the same method used to calculate $IAP_{Dolomite}$ according to Equations (23) and (24).



$$IAP_{Calcite} = [a_{Ca^{2+}}][a_{CO_3^{2-}}], \quad (22)$$



$$IAP_{Dolomite} = [a_{Ca^{2+}}][a_{Mg^{2+}}][a_{CO_3^{2-}}]^2. \quad (24)$$

On the basis of the above equations and concentrations of Ca^{2+} , Mg^{2+} , and CO_3^{2-} , the IAP values for calcite and dolomite were calculated, respectively. The $\log IAP_{dolomite}$ values along the two sampling lines were greater than $\log K_{sp-dolomite}$, whereas the $IAP_{calcite}$ values were greater than $\log K_{sp-calcite}$ at shallow hydraulic head, due to DIC generated by AOM (Figure 10). In the study area, the relative sizes of IAP and K_{sp} illustrated the possibility of authigenic carbonate precipitation, because of AOM by sulfate reducing bacteria at the specific hydraulic head.

Furthermore, the software program PHREEQC was used to assess evaluate the carbonate system in which the saturation index (SI) is calculated as Equation (25):

$$SI = \log(IAP/K_S(T)) \quad (25)$$

where $K_S(T)$ is the mineral equilibrium constant under in 25 °C conditions. An SI greater than 0 indicates the mineral phase under precipitation or oversaturation state, whereas an SI less than 0 indicates the mineral phase under unsaturation or dissolution state [50].

On the basis of the saturation index of calcite ($SI_{calcite}$) and dolomite ($SI_{dolomite}$) together with hydraulic head (H), as shown in Figure 11, the positive values of $SI_{dolomite}$ demonstrate that the dolomite precipitation was thermodynamically favored in the study area, whereas the plot of $SI_{calcite}$ values against H suggest that calcite was oversaturated at the shallower depth and close to undersaturation at the deeper depth in the coalbed reservoir water [51]. The results of PHREEQC agree with above analysis, providing a strong support for the state of these carbonate minerals.

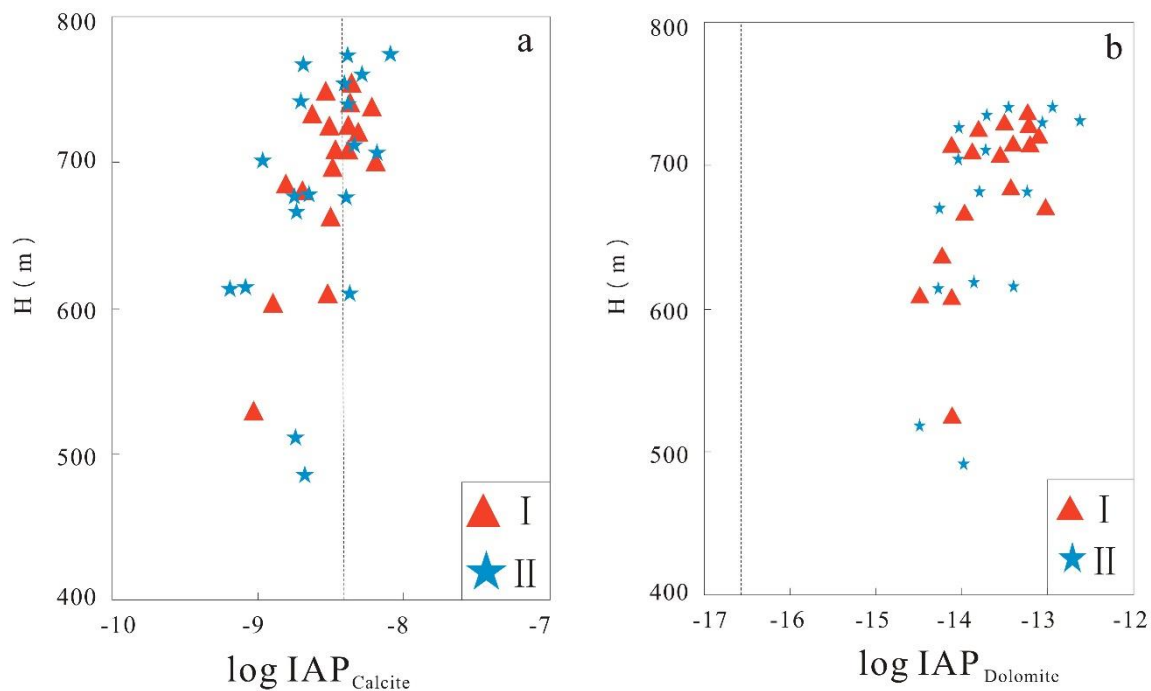


Figure 10. Depth profiles of log IAP for (a) calcite and (b) dolomite calculated using the Ca^{2+} , Mg^{2+} , and CO_3^{2-} concentrations in water samples with hydraulic head (H). Dashed lines represent $\log K_{\text{sp-Calcite}}$ and $\log K_{\text{sp-Dolomite}}$.

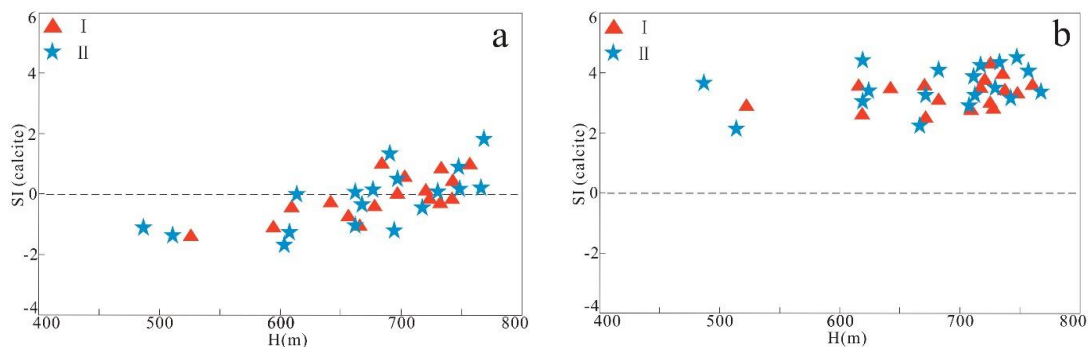


Figure 11. Plots of saturation index (SI) for (a) calcite and (b) dolomite against H in the Shizhuangnan block.

5. Conclusions

The major ion distributions, isotopic compositions, and 16S rRNA analysis reflect the geochemical characteristics of CBM co-produced water from the Shizhuangnan block and provide important information to understand the biogeochemistry of the coal reservoir water system. The following conclusions have been drawn:

1. The chemical compositions of the CBM co-produced water along flow paths were controlled by various degrees of mineral weathering such as silicate, gypsum, and sulphide, as well as exchange of Ca^{2+} and Mg^{2+} for Na^+ (K^+). Carbon and hydrogen isotopes of the dissolved methane combined with positive $\delta^{13}\text{C}_{\text{DIC}}$ values, hydrogen, and oxygen isotopes in the coal reservoir water strongly indicated the occurrence of methanogenesis.
2. Sulfate reduction was the main reason for sulfate decrease, accompanied by hydraulic head change, as confirmed by 16S rRNA analysis, and sulfate was mostly consumed by anaerobic oxidation of methane in the study area. Due to the competition between sulfate-reducing bacteria

and methanogens, methanogens tended to be more active at deeper hydraulic head in the coal reservoir water.

- There were significant differences in the abundance and distribution of methanogens and sulfate-reducing bacteria at different hydraulic heads. Most of the methanogens detected belonged to *Methanobacteriales*, representing a methanogenesis type of CO₂ reduction.
- A large amount of DIC produced by sulfate-reducing bacteria strengthened dolomite and calcite precipitation, as shown by comparing the relative sizes of K_{sp} and IAP.

Author Contributions: Conceptualization, Y.L. and S.T.; methodology, Y.L.; validation, Y.L. and S.Z.; formal analysis, Z.X.; investigation, P.W.; resources, S.T.; writing—original draft preparation, Y.L.; writing—review and editing, Y.L.; supervision, S.Z. and Z.X.; project administration, S.T.; funding acquisition, S.T. All authors have read and agreed to the published version of the manuscript.

Funding: This work was supported by the National Natural Science Foundation of China (grant number 41772159/D0208; grant number 41872178; grant number U1910205), the National Science and Technology Major Project of China (grant number 2017ZX05064003) and the Fundamental Research Funds for the Central Universities (grant number 2652018233).

Acknowledgments: We would like to thank China United Coalbed Methane Corporation for providing the production well date.

Conflicts of Interest: No conflict of interest exists in the submission of this manuscript, and the manuscript was approved by all authors for publication.

References

- Moore, T.A. Coalbed methane: A review. *Int. J. Coal Geol.* **2012**, *101*, 36–81. [[CrossRef](#)]
- Owen, D.D.R.; Raiber, M.; Cox, M.E. Relationships between major ions in coal seam gas groundwaters: Examples from the Surat and Clarence-Moreton basins. *Int. J. Coal Geol.* **2015**, *137*, 77–91. [[CrossRef](#)]
- Pashin, J.C.; McIntyre-Redden, M.R.; Mann, S.D.; Kopaska-Merkel, D.C.; Varonka, M.; Orem, W. Relationships between water and gas chemistry in mature coalbed methane reservoirs of the Black Warrior Basin. *Int. J. Coal Geol.* **2014**, *126*, 92–105. [[CrossRef](#)]
- Huang, H.Z.; Bi, C.Q.; Sang, S.X.; Miao, Y.; Zhang, H.J. Signature of coproduced water quality for coalbed methane development. *J. Nat. Gas Sci. Eng.* **2017**, *47*, 34–46. [[CrossRef](#)]
- Papendick, S.L.; Downs, K.R.; Vo, K.D.; Hamilton, S.K.; Dawson, G.K.W.; Golding, S.D.; Gilcrease, P.C. Biogenic methane potential for Surat Basin, Queensland coal seams. *Int. J. Coal Geol.* **2011**, *88*, 123–134. [[CrossRef](#)]
- Luo, G.; Algeo, T.J.; Zhan, R.; Yan, D.; Huang, J.; Liu, J.; Xie, S. Perturbation of the marine nitrogen cycle during the Late Ordovician glaciation and mass extinction. *Palaeogeogr. Palaeoclimatol.* **2016**, *448*, 339–348. [[CrossRef](#)]
- Guo, H.G.; Yu, Z.S.; Zhang, H.X. Phylogenetic diversity of microbial communities associated with coalbed methane gas from Eastern Ordos Basin, China. *Int. J. Coal Geol.* **2015**, *150–151*, 120–126. [[CrossRef](#)]
- Hinrichs, K.U.; Hayes, J.M.; Sylva, S.P.; Brewer, P.G.; DeLong, E.F. Methane-consuming archaeobacteria in marine sediments. *Nature* **1999**, *398*, 802–805. [[CrossRef](#)]
- Luo, G.; Kump, L.R.; Wang, Y.; Tong, J.; Arthur, M.A.; Yang, H.; Huang, J.; Yin, H.; Xie, S. Isotopic evidence for an anomalously low oceanic sulfate concentration following end-Permian mass extinction. *Earth Planet. Sci. Lett.* **2010**, *300*, 101–111. [[CrossRef](#)]
- Hong, W.L.; Torres, M.E.; Kim, J.H.; Choi, J.; Bahk, J.J. Towards quantifying the reaction network around the sulfate–methane–transition-zone in the Ulleung Basin, East Sea, with a kinetic modeling approach. *Geochim. Cosmochim. Acta* **2014**, *140*, 127–141. [[CrossRef](#)]
- Komada, T.; Burdige, D.J.; Li, H.L.; Magen, C.; Chanton, J.P.; Cada, A.K. Organic matter cycling across the sulfate–methane transition zone of the Santa Barbara Basin, California Borderland. *Geochim. Cosmochim. Acta* **2016**, *176*, 259–278. [[CrossRef](#)]
- Li, Q.G.; Ju, Y.W.; Lu, W.Q.; Wang, G.C.; Neupane, B.; Sun, Y. Water–rock interaction and methanogenesis in formation water in the southeast Huaibei coalfield, China. *Mar. Pet. Geol.* **2016**, *77*, 435–447. [[CrossRef](#)]

13. Luo, G.; Hallmann, C.; Xie, S.; Ruan, X.; Summons, R.E. Comparative microbial diversity and redox environments of black shale and stromatolite facies in the Mesoproterozoic Xiamaling Formation. *Geochim. Cosmochim. Acta* **2015**, *151*, 150–167. [[CrossRef](#)]
14. Zhang, Z.; Qin, Y.; Bai, J.P.; Li, G.Q.; Zhuang, X.G.; Wang, X.M. Hydrogeochemistry characteristics of produced waters from CBM wells in Southern Qinshui Basin and implications for CBM commingled development. *J. Nat. Gas Sci. Eng.* **2018**, *56*, 428–443. [[CrossRef](#)]
15. Guo, H.G.; Yu, Z.S.; Thompson, I.P.; Zhang, H.X. A contribution of hydrogenotrophic methanogenesis to the biogenic coal bed methane reserves of Southern Qinshui Basin, China. *Appl. Microbiol. Biotechnol.* **2014**, *98*, 9083–9093. [[CrossRef](#)]
16. Yang, X.Q.; Chen, Y.M.; Wu, R.W.; Nie, Z.Q.; Han, Z.Y.; Tan, K.L.; Chen, L.Y. Potential of biogenic methane for pilot-scale fermentation ex situ with lump anthracite and the changes of methanogenic consortia. *J. Ind. Microbiol. Biotechnol.* **2018**, *45*, 229–237. [[CrossRef](#)]
17. Wang, B.; Sun, F.; Tang, D.; Zhao, Y.; Song, Z.; Tao, Y. Hydrological control rule on coalbed methane enrichment and high yield in FZ block of Qinshui Basin. *Fuel* **2015**, *140*, 568–577. [[CrossRef](#)]
18. Li, Y.; Shi, W.; Tang, S.H. Microbial Geochemical Characteristics of the Coalbed Methane in the Shizhuangnan Block of Qinshui Basin, North China and their Geological Implications. *Acta. Geol. Sin-Engl.* **2019**, *93*, 660–674. [[CrossRef](#)]
19. Zhang, J.Y.; Liu, D.M.; Cai, Y.D.; Pan, Z.J.; Yao, Y.B.; Wang, Y.J. Geological and hydrological controls on the accumulation of coalbed methane within the No. 3 coal seam of the southern Qinshui Basin. *Int. J. Coal Geol.* **2017**, *182*, 94–111. [[CrossRef](#)]
20. Tao, S.; Tang, D.Z.; Xu, H.; Gao, L.; Fang, Y. Factors controlling high-yield coalbed methane vertical wells in the Fanzhuang Block, Southern Qinshui Basin. *Int. J. Coal Geol.* **2014**, *134–135*, 38–45. [[CrossRef](#)]
21. Yao, Y.B.; Liu, D.M.; Yan, T. Geological and hydrogeological controls on the accumulation of coalbed methane in the Weibei field, southeastern Ordos Basin. *Int. J. Coal Geol.* **2014**, *121*, 148–159. [[CrossRef](#)]
22. Guo, P.K.; Cheng, Y.P.; Jin, K.; Liu, Y.P. The impact of faults on the occurrence of coal bed methane in Renlou coal mine, Huaibei coalfield, China. *J. Nat. Gas Sci. Eng.* **2014**, *17*, 151–158. [[CrossRef](#)]
23. Jiang, B.; Qu, Z.; Wang, G.G.X.; Li, M. Effects of structural deformation on formation of coalbed methane reservoirs in Huaibei coalfield, China. *Int. J. Coal Geol.* **2010**, *82*, 175–183. [[CrossRef](#)]
24. Wang, X.; Jiao, Y.; Wu, L.; Rong, H.; Wang, X.; Song, J. Rare earth element geochemistry and fractionation in Jurassic coal from Dongsheng-Shenmu area, Ordos Basin. *Fuel* **2014**, *136*, 233–239. [[CrossRef](#)]
25. Gao, L.; Brassell, S.C.; Mastalerz, M.; Schimmelmann, A. Microbial degradation of sedimentary organic matter associated with shale gas and coalbed methane in eastern Illinois Basin. *Int. J. Coal Geol.* **2013**, *107*, 152–164. [[CrossRef](#)]
26. Cai, Y.D.; Liu, D.M.; Yao, Y.B.; Li, J.; Qiu, Y. Geological controls on prediction of coalbed methane of No. 3 coal seam in Southern Qinshui Basin, North China. *Int. J. Coal Geol.* **2011**, *88*, 101–112. [[CrossRef](#)]
27. Li, Q.G.; Ju, Y.W.; Bao, Y.; Yan, Z.F.; Li, X.S.; Sun, Y. Composition, Origin, and Distribution of Coalbed Methane in the Huaibei Coalfield, China. *Energy Fuels* **2015**, *29*, 546–555. [[CrossRef](#)]
28. Shen, Y.A.; Buick, R.; Canfield, D.E. Isotopic evidence for microbial sulphate reduction in the early Archaean era. *Nature* **2001**, *410*, 77–81. [[CrossRef](#)]
29. Zabel, M.; Schulz, H.D. Importance of submarine landslides for non-steady state conditions in pore water system-lower Zaire (Congo) deep-sea fan. *Mar. Geol.* **2001**, *176*, 87–99. [[CrossRef](#)]
30. Meister, P.; McKenzie, J.A.; Vasconcelos, C.; Bernasconi, S.; Frank, M.; Gutjahr, M.; Schrag, D.P. Dolomite formation in the dynamic deep biosphere: Results from the Peru Margin. *Sedimentol.* **2007**, *54*, 1007–1031. [[CrossRef](#)]
31. Warthmann, R.; Van, L.Y.; Vasconcelos, C.; McKenzie, J.A.; Karpoff, A. Bacterially induced dolomite precipitation in anoxic culture experiments. *Geology* **2000**, *28*, 1091–1094. [[CrossRef](#)]
32. Luo, G.; Junium, C.K.; Kump, L.R.; Huang, J.; Li, C.; Feng, Q.; Shi, X.; Bai, X.; Xie, S. Shallow stratification prevailed for 1700 to 1300 Ma ocean: Evidence from organic carbon isotopes in the North China Craton. *Earth Planet. Sci. Lett.* **2014**, *400*, 219–232. [[CrossRef](#)]
33. Sharma, S.; Baggett, J.K. Application of carbon isotopes to detect seepage out of coalbed natural gas produced water impoundments. *Appl. Geochem.* **2011**, *26*, 1423–1432. [[CrossRef](#)]

34. Bates, B.L.; McIntosh, J.C.; Lohse, K.A.; Brooks, P.D. Influence of groundwater flowpaths, residence times and nutrients on the extent of microbial methanogenesis in coal beds: Powder River Basin, USA. *Chem. Geol.* **2011**, *284*, 45–61. [[CrossRef](#)]
35. Schlegel, M.E.; McIntosh, J.C.; Bates, B.L.; Kirk, M.F.; Martini, A.M. Comparison of fluid geochemistry and microbiology of multiple organic-rich reservoirs in the Illinois Basin, USA: Evidence for controls on methanogenesis and microbial transport. *Geochim. Cosmochim. Acta* **2011**, *75*, 1903–1919. [[CrossRef](#)]
36. Zhang, S.H.; Tang, S.H.; Li, Z.C.; Guo, Q.L.; Pan, Z.J. Stable isotope characteristics of CBM co-produced water and implications for CBM development: The example of the Shizhuangnan block in the southern Qinshui Basin, China. *J. Nat. Gas Sci. Eng.* **2015**, *27*, 1400–1411. [[CrossRef](#)]
37. Golding, S.D.; Boreham, C.J.; Esterle, J.S. Stable isotope geochemistry of coal bed and shale gas and related production waters: A review. *Int. J. Coal Geol.* **2013**, *120*, 24–40. [[CrossRef](#)]
38. Hamilton, S.K.; Golding, S.D.; Baublys, K.A.; Esterle, J.S. Stable isotopic and molecular composition of desorbed coal seam gases from the Walloon Subgroup, eastern Surat Basin, Australia. *Int. J. Coal Geol.* **2014**, *122*, 21–36. [[CrossRef](#)]
39. Fallgren, P.H.; Jin, S.; Zeng, C.; Ren, Z.; Lu, A.; Colberg, P.J.S. Comparison of coal rank for enhanced biogenic natural gas production. *Int. J. Coal Geol.* **2013**, *115*, 92–96. [[CrossRef](#)]
40. Jones, E.J.P.; Voytek, M.A.; Corum, M.D.; Orem, W.H. Stimulation of methane generation from nonproductive coal by addition of nutrients or a microbial consortium. *Appl. Environ. Microbiol.* **2010**, *76*, 7013–7022. [[CrossRef](#)]
41. Ghosh, S.; Golding, S.D.; Varma, A.K.; Baublys, K.A. Stable isotopic composition of coal bed gas and associated formation water samples from Raniganj Basin, West Bengal, India. *Int. J. Coal Geol.* **2018**, *191*, 1–6. [[CrossRef](#)]
42. Meslé, M.; Dromart, G.; Oger, P. Microbial methanogenesis in subsurface oil and coal. *Res. Microbiol.* **2013**, *164*, 959–972. [[CrossRef](#)]
43. Robbins, S.J.; Evans, P.N.; Esterle, J.S.; Golding, S.D.; Tyson, G.W. The effect of coal rank on biogenic methane potential and microbial composition. *Int. J. Coal Geol.* **2016**, *154–155*, 205–212. [[CrossRef](#)]
44. Colosimo, F.; Thomas, R.; Lloyd, J.R.; Taylor, K.G.; Boothman, C.; Smith, A.D.; Lord, R.; Kalin, R.M. Biogenic methane in shale gas and coal bed methane: A review of current knowledge and gaps. *Int. J. Coal Geol.* **2016**, *165*, 106–120. [[CrossRef](#)]
45. Chen, F.; He, H.; Zhao, S.M.; Yao, J.H.; Sun, Q.; Huang, G.H.; Xiao, D.; Tang, L.F.; Leng, Y.W.; Tao, X.X. Analysis of microbial community succession during methane production from Baiyinhua lignite. *Energy Fuels* **2018**, *32*, 10311–10320. [[CrossRef](#)]
46. Bao, Y.; Ju, Y.; Huang, H.P.; Yun, J.L.; Guo, C. Potential and constraints of biogenic methane generation from coals and mudstones from Huaibei coalfield, eastern China. *Energy Fuels* **2019**, *33*, 287–295. [[CrossRef](#)]
47. Mazzini, A.; Svensen, H.; Hovland, M.; Planke, S. Comparison and implications from strikingly different authigenic carbonates in a Nyegga complex pockmark, G11, Norwegian Sea. *Mar. Geol.* **2006**, *231*, 89–102. [[CrossRef](#)]
48. Wehrmann, L.M.; Risgaard-Petersen, N.; Schrum, H.N.; Walsh, E.A.; Huh, Y.; Ikehara, M. Coupled organic and inorganic carbon cycling in the deep seafloor sediment of the northeastern Bering Sea Slope. The Integrated Ocean Drilling Program Expedition 323 Scientific Party. *Chem. Geol.* **2011**, *284*, 251–261. [[CrossRef](#)]
49. Moore, T.S.; Murray, R.W.; Kurtz, A.C.; Schrag, D.P. Anaerobic methane oxidation and the formation of dolomite. *Earth Planet. Sci. Lett.* **2004**, *229*, 141–154. [[CrossRef](#)]
50. Qian, C.; Wu, X.; Mu, W.P.; Fu, R.Z.; Zhu, G.; Wang, Z.R.; Wang, D.D. Hydrogeochemical characterization and suitability assessment of groundwater in an agro-pastoral area, Ordos Basin, NW China. *Environ. Earth Sci.* **2016**, *75*, 20. [[CrossRef](#)]
51. Qian, J.Z.; Wang, L.; Ma, L.; Lu, Y.H.; Zhao, W.D.; Zhang, Y. Multivariate statistical analysis of water chemistry in evaluating groundwater geochemical evolution and aquifer connectivity near a large coal mine, Anhui, China. *Environ. Earth Sci.* **2016**, *75*, 9. [[CrossRef](#)]

